

**ELECTROPHYSIOLOGICAL AND BEHAVIORAL TESTING REVEAL
ABERRANT VISUAL PROCESSING IN *SYNGAP1*+/- MICE**

by

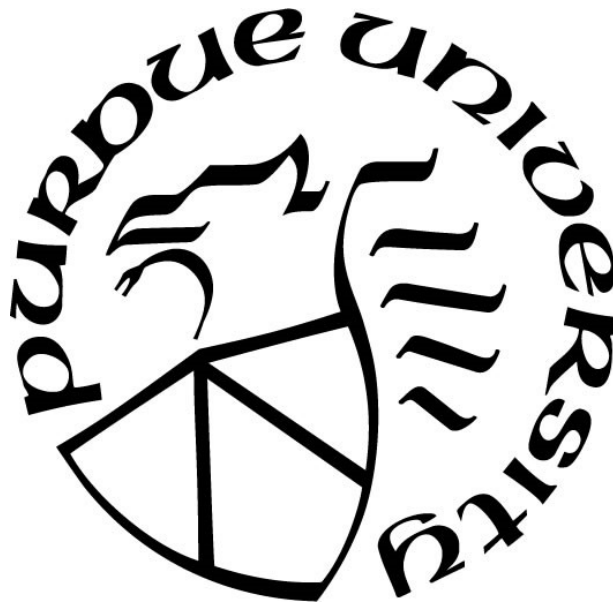
Charles Andrew Martin

A Thesis

Submitted to the Faculty of Purdue University

In Partial Fulfillment of the Requirements for the degree of

Master of Science in Biomedical Engineering



Weldon School of Biomedical Engineering

West Lafayette, Indiana

May 2022

**THE PURDUE UNIVERSITY GRADUATE SCHOOL
STATEMENT OF COMMITTEE APPROVAL**

Dr. Maria Dadarlat Makin, Chair

Weldon School of Biomedical Engineering

Dr. Tamara Kinzer-Ursem

Weldon School of Biomedical Engineering

Dr. Estuardo Robles

Department of Biological Sciences

Approved by:

Dr. Tamara Kinzer-Ursem

*To Eleanor Rose Clifton who was my rock throughout the process of preparing this thesis.
Without you there to listen to me grumble about debugging Matlab code, this thesis would have
been immeasurably harder to write.
Also, to my parents and family who have always supported me throughout my academic career.*

ACKNOWLEDGMENTS

Throughout my time working on this thesis, I have received a wide range of support from many people within the Purdue BME community.

Most importantly, I would like to thank my amazing advisor Dr. Maria Dadarlat. Your insight into neural recording techniques and statistical analysis were invaluable resources in keeping me zoned in on my research. You also made sure to consistently push me to widen my abilities as a researcher and critical thinker.

Megan Lipton, your help in keeping me sane in lab throughout the thesis process was invaluable. Without your help it is highly likely I would never have figured out how to order any supplies for the lab.

Evan Anderson, your assistance over the summer was critical in the development of the receptive field sizing analysis. Without your assistance, this analysis step would not have been as well designed.

To the rest of the lab members of the Dadarlat Lab - especially Seungbin Park, Ramya Banda, Luz Andrino, and Brenna Vaughn – thank you for your encouragement and support throughout the thesis process. This support helped the long experiment and writing hours fly by much too quickly.

Dr. Wendy Koss and Dr. Kaisa Ejendal, your assistance was invaluable throughout the development of my thesis. Wendy, thank you for assisting me with the development of my behavioral experiment and in guiding my use of the resources in the Behavioral Core to their fullest. Kaisa, thank you for providing guidance on mouse genetics and in assisting me in acquiring mice on short notice for experiments.

TABLE OF CONTENTS

LIST OF TABLES	8
LIST OF FIGURES	9
ABSTRACT.....	11
1. INTRODUCTION	12
1.1 Visual Development.....	12
1.2 Single Neuron Anatomy	13
1.3 Role of SynGAP in the Synapse	13
1.4 Transgenic (<i>Syngap1</i> ^{+/-}) Mutant Mice	14
1.5 Loss of Function <i>SYNGAP1</i> Mutations in Humans	15
1.6 Behavioral Deficits in <i>Syngap1</i> ^{+/-} Mice	15
1.7 Hypothesis for Electrophysiology in the Visual System of <i>Syngap1</i> ^{+/-} Mice	16
2. METHODS	18
2.1 Mouse Model Information	18
2.2 Surgeries	18
2.2.1 Headplate Surgeries	18
2.2.2 Craniotomies.....	19
2.3 Electrophysiological System and Head Fixed Recordings	20
2.3.1 Ephys System Description.....	20
2.3.2 Head Fixed Recording Setup and Procedure	21
2.4 Visual Stimulation	22
2.4.1 Monocular.....	23
2.4.2 Binocular.....	23
2.5 Behavioral Experiments.....	24

2.5.1	Citric Acid Water Conditioning.....	24
2.5.2	Behavioral Experiment Setup and Equipment.....	24
2.5.3	Behavioral Experiment Pretraining	24
2.5.4	Adaptive Pairwise Visual Discrimination (APD) Task.....	27
2.5.5	Mouse Activity Boxes	27
2.6	Electrophysiological Recording Analysis.....	27
2.6.1	Electrophysiological Data Preparation Process	27
2.6.2	Receptive Field Sizing.....	28
2.6.3	Tuning Curve Isolation	28
2.6.4	Orientation Selectivity Index and Circular Variance.....	28
2.6.5	Neuronal Firing Rate	30
2.6.6	Ocular Dominance Index.....	30
2.6.7	d-Prime Analysis	31
2.7	Behavioral Data Analysis	32
2.7.1	Open Field Activity Analysis	32
2.7.2	APD Data Analysis.....	32
3.	RESULTS.....	34
3.1	Receptive field spread remained similar among wild type and <i>Syngap1</i> ^{+/-} neurons.....	34
3.2	Orientation selectivity was reduced in <i>Syngap1</i> ^{+/-} mice	34
3.3	Tuned <i>Syngap1</i> ^{+/-} neurons demonstrate a depressed firing rate.....	35
3.4	No significant differences in binocular matching detected through the ODI.....	36
3.5	Population level analysis indicates differences in neural responses.....	37
3.6	<i>Syngap1</i> ^{+/-} mice exhibit increased hyperactivity and impulsivity	38
3.7	<i>Syngap1</i> ^{+/-} mice had difficulty discriminating finer angles	40
4.	DISCUSSION AND CONCLUSIONS.....	41

REFERENCES 44

LIST OF TABLES

Table 1: Pretraining and APD Task Regimen Outline..... 26

LIST OF FIGURES

Figure 1: Developmental schedule of the visual system with indications of when early maturation of synapses occurs in <i>Syngap1</i> +/- mice.....	14
Figure 2: The custom headplate and headplate holder used for craniotomies.....	19
Figure 3: Acute electrophysiological recording setup. The mouse is headplated with an acute recording probe inserted into V1 and allowed to run freely on either a KineMouse wheel or styrofoam running ball. Visual stimuli on screens are placed in the visual field of the mouse during the experiment. Not shown are the Intan recording board, binocular shutters, and peripheral support equipment. *This brain image was generated from the Allen Mouse Brain Connectivity Atlas using the 3D brain explorer [29], [30].....	21
Figure 4: Examples of drifting grating and receptive field stimuli.....	23
Figure 5: Angle incrementation for the APD task. a) Correct stimulus always remains at 90°. b) Incorrect stimulus begins at 0° and increments by 2.5° towards 90°	27
Figure 6: Example of OSI calculations in reference to a sinusoidal example tuning curve	29
Figure 7: Example of how CV demonstrates neuronal tuning in reference to example tuning curves	30
Figure 8: Examples of discrimination ability between two angles for a neuron with high and low d' values.....	32
Figure 9: a) Examples of receptive and non-receptive fields in <i>Syngap1</i> +/- and wild type mice. b) Spread of receptive field selectivity (p = 0.2894).....	34
Figure 10: a) Examples of specific and non-specific tuning curves from wild type littermate controls and <i>Syngap1</i> +/- mice. b) Tuning curve OSI (p = 0.0013) and CV (p = 0.0287) histograms.....	35
Figure 11: Histograms of firing rates for monocular recording neurons. a) Overall firing rate of all neurons over the 0.2 Hz threshold (p = 0.5166). b) Firing rate of tuned and untuned neurons (Tuned: p = 8.2081e-12, Untuned: p = 0.9165).....	36
Figure 12: Histograms demonstrating binocular matching responses of neurons. a) ODI Response (p = 0.1544). b) Difference in preferred direction (p = 0.1864)	37
Figure 13: d' analysis of neurons. p = 7.6337 X 10 ⁻⁵⁰	38
Figure 14: Results from the open field activity of <i>Syngap1</i> +/- and littermate controls. a) SuperFlex Open Field System. b) Heatmap of movement around cage for mice separated by, and average across the mouse genotype. c-g) Mobility metrics compared between the two genotypes utilizing a Wilcoxon rank sum test.....	39
Figure 15: Average latency response to select correct stimulus after initiation of the trial. The stars indicate training sessions where a Wilcoxon rank sum test found significance of p < 0.05. 39	39

Figure 16: APD task demonstration of long-term task learning and statistical differences in the discrimination threshold of *Syngap1*^{+/-} mice and wild type controls..... 40

ABSTRACT

Syngap1^{+/-} is a mouse model for intellectual disability and autism spectrum disorder where haploinsufficiency of the *Syngap1* gene and therefore downregulation of SynGAP1 leads to early maturation of synapses within the brain within post-natal days fourteen and sixteen instead of at the normal developmental schedule of post-natal day thirty. This early-shifted timeline falls directly before the visual critical where binocular matching between inputs from the two eyes occurs, and during a period where neurons become selective to specific orientations. High-level visual and cognitive issues observed in autism spectrum disorder patients might follow from deficits in basic sensory processing development, but it is not yet understood how *Syngap1* haploinsufficiency affects visual development and visual processing. Therefore, to characterize visual processing within the *Syngap1*^{+/-} mouse model of autism spectrum disorder, acute electrophysiological recordings were performed within the monocular and binocular regions of the mouse visual cortex (V1). Responses to a series of visual stimuli were analyzed to measure and compare receptive field size, orientation selectivity, and binocularity between *Syngap1*^{+/-} mice and littermate controls. In order to understand how potential deficits in physiology could translate into visual perception, a behavioral training protocol was implemented which isolated visual acuity in mice. In accordance with known developmental timelines in the visual cortex, it was found that the receptive field sizes of V1 neurons in *Syngap1*^{+/-} mice were unchanged from wild type controls. However, these same neurons had wider tuning curves and lower firing rates than neurons in littermate controls. Ocular dominance was unaltered between *Syngap1*^{+/-} and wild type mice, but this was possibly due to low sample sizes of neurons from the binocular regions of V1. At the behavioral level, lower visual acuities were discovered in *Syngap1*^{+/-} mice with a size degree difference compared to littermate controls – a minor but significant difference. These results indicate a reduction in SynGAP1 expression has a perceivable effect on V1 development and function at both physiological and behavioral levels.

1. INTRODUCTION

1.1 Visual Development

Refinement of the mouse and human visual systems occurs over a series of prolonged stages. While the human visual system takes many years for full development and refinement, the mouse visual system develops much more quickly due to the differences in lifespan [1], [2]. This shortened developmental timeline, along with genetic tools make mouse models optimal for understanding the effects of genetic mutations on visual system function [3].

The mouse visual system has three major developmental stages which are critical in the development of coherent visual cortex responses to visual stimuli. During the first stage, retinotopy begins to be expressed. Retinotopy is when projections from the retina through the dorsal lateral geniculate nucleus (dLGN) to the primary visual cortex (V1) create a cohesive mapping of the visual field in V1 [2]. This cohesive map ensures that neurons in V1 will only respond to specific portions of the mouse's visual field.

The second stage of visual system development is the refinement of orientation selectivity. Orientation selectivity is where neurons begin to develop a stronger response to a specific orientation of a stimulus compared to all other orientations [2]. As the development of orientation selectivity corresponds with eye opening, visual experience serves to refine and maintain orientation selectivity but is not a requirement to promote the development of orientation selectivity [2], [4]. Direction selectivity, or the specificity of a neuron to a specific direction of movement of a visual stimulus, is developed in the same time period as orientation selectivity [4].

The critical period of binocular matching from post-natal days 21 to 35 (P21-P35) corresponds with the third major period of development in the visual system. Initially in the developmental pathway, neuronal responses to oriented visual stimuli from the two eyes are originally different based on if the stimulus is received from the ipsilateral or contralateral eye [2]. During the critical period, as connections are pruned and reinforced from visual experience, the orientation preference of binocular neurons shifts to obtain the same preferred orientation for stimuli from either eye [2]. This binocularity is retained after the closure of the critical period and is expressed throughout the animal's life. Alongside these three critical aspects of visual development, connections to higher visual areas (HVAs) are continuously refined throughout this time period, beginning at P7 [5].

1.2 Single Neuron Anatomy

Neural signaling leads to the development of synaptic plasticity due to the process by which signals are transmitted within and between neurons. Within the neurons, neural information is transmitted through an ion flux down from the dendrites where a signal is received and through to the axon [6]. Upon reaching the axon, the signal moves into the synapses where the release of chemical neurotransmitters controls the stimulation of the next synapse and the corresponding electrical signal response in the next neuron [6]. This region on the surface of the synapse is known as the post synaptic density (PSD) due to the high concentration of proteins which regulate neural signaling and allow for optimized neurotransmitter release. When continued potentiation of a specific neural pathway through synapse occurs, the neuron's synapses are altered to allow for strengthening of synaptic signaling. While there are multiple mechanisms to control this plastic response and they are not fully understood, two major methods of plastic development are AMPAR insertion onto the synapse and physical synapse enlargement [7].

1.3 Role of SynGAP in the Synapse

Synaptic Ras GTPase activating protein (SynGAP) is a highly abundant protein within the PSD of neurons in the brain [7]–[9]. Specifically, SynGAP1 expression within the brain is chiefly localized to the hippocampus, cortex, and striatum by P56 [9]. However, during development SynGAP1 is primarily concentrated in the cytosol up until P14-P21 where expression of the SynGAP1- α 1 isoform becomes upregulated [9]. Throughout this period, SynGAP expression shifts to become largely concentrated in the PSD. This localization of SynGAP to the PSD allows SynGAP to act as a major mediator of synaptic plasticity by regulating Ras and Rap activity within the synapse and the inactivation through phosphorylation of cofilin, an actin-severing protein [7], [10], [11].

Specifically, following N-methyl-D-aspartate receptor (NMDAR) dependent long-term potentiation (LTP) SynGAP is phosphorylated by CaMKII leading to a decreased SynGAP binding affinity to postsynaptic density protein 95 (PSD-95). This reduced binding affinity to PSD-95 allows for rapid diffusion of SynGAP- α 1 from the PSD unlocking the breaks on the Ras and Rap signaling pathways [12]. This allows for downstream AMPAR insertion on the synapse which strengthens the synaptic connection between neurons [7], [10]. Additionally, the removal of

SynGAP from the PSD decreases its ability to regulate steady-state phosphorylation of cofilin and NMDAR activated transient cofilin activation [11]. Spine enlargement, and therefore an increased signaling response, develops due to the activation of cofilin by the removal of SynGAP controlled phosphorylation which allows for the promotion of actin polymerization [11].

1.4 Transgenic (*Syngap1*^{+/-}) Mutant Mice

Due to the critical role SynGAP plays in the regulation of synaptic plasticity and maturation of neurons, the reduced levels of SynGAP expression in the brain drives synaptic, neuronal circuit, structural, and behavioral changes. On the synapse level, *Syngap1*^{+/-} mice demonstrate deficits in LTP especially in relation to spike pairing and theta burst stimulation [7]. Additionally, an increase in the number of mushroom spines in the hippocampus has been observed in *Syngap1*^{+/-} mice [11]. While no circuit organizational changes to the visual cortex have been observed, reductions in whisker barrel segregation in the somatosensory cortex have been identified [13]. In *Syngap1* heterozygous mice, the reduced expression of SynGAP1 results in the early maturation of synaptic spines around P14-P16 [14], [15]. This time period corresponds with the shift in SynGAP concentration from the cytosol to the PSD discussed above and the beginning of the process of orientation selectivity development (Figure 1) in V1 [2], [9]. Because this lack of SynGAP drives the early maturation of spines before the visual critical period where binocular matching occurs, it is likely this alteration of SynGAP levels serves to drive the early closing of visual critical periods.

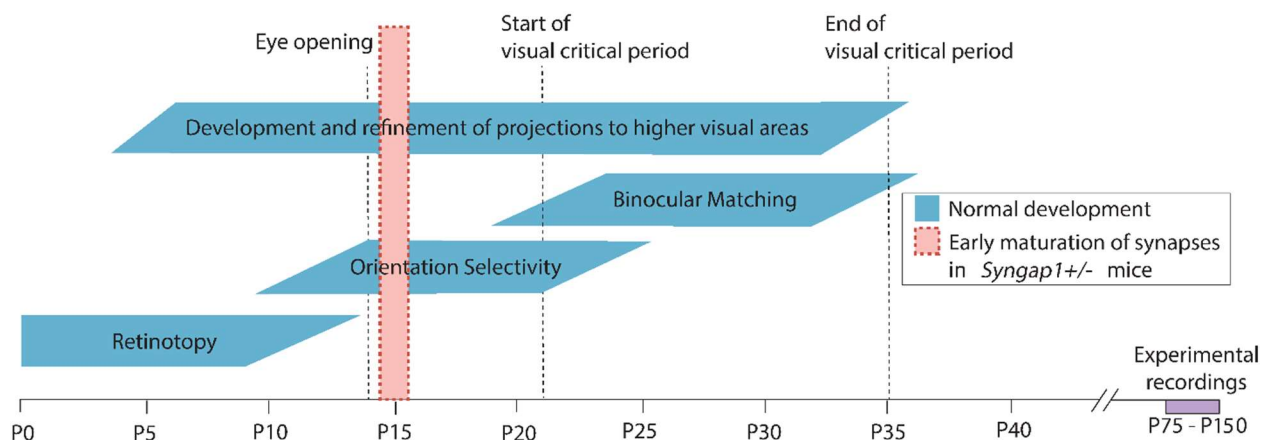


Figure 1: Developmental schedule of the visual system with indications of when early maturation of synapses occurs in *Syngap1*^{+/-} mice

SYNGAP1 mutations have been demonstrated to be a possible cause of intellectual disability (ID) and autism spectrum disorder (ASD) alongside other neurodevelopmental disorders such as schizophrenia and epilepsy [16], [17]. Additionally, for ID, ASD, and epilepsy patients, *SYNGAP1* mutations have been directly isolated through genetic analyses as major contributors to these conditions [17], [18]. The majority of these ID and ASD phenotypes were caused by *SYNGAP1* loss of function variants where reduced protein expression or altered protein function – leading to what is essentially reduced protein expression – is equitable to *Syngap1*^{+/-} mouse models [18].

1.5 Loss of Function *SYNGAP1* Mutations in Humans

In humans, *SYNGAP1* mutations affect cognitive function, learning and developmental delays, neuronal excitatory balance changes leading to seizures, sleeping problems, and aggression [7], [17]. Additionally, children with a *SYNGAP1* de novo mutation often do not walk without aid until after 3 years of age. Reduced responses to pain and increased risk-taking behaviors have been reported from studies with *SYNGAP1* patients [19], [20]. Gross brain morphology changes have also been observed in some specific populations of patients with severe de novo variants of *SYNGAP1* where minor microcephaly is evident [19], [21], [22]. In some patients (30%) brain region specific changes have been detected through MRI imaging, however these changes have not been fully quantified [19]. Additionally, studies of neural activities in ASD patients have found alterations in visual processing including in relation to the primary visual cortex [23].

1.6 Behavioral Deficits in *Syngap1*^{+/-} Mice

Animals presenting *Syngap1* haploinsufficiency have been shown to develop many behavioral traits consistent with ID and ASD. *Syngap1* heterozygous mice develop hyperactive behavior and show increased impulsivity in behavioral tasks [17], [24]. In visual discrimination tasks with eventual reversal learning, *Syngap1*^{+/-} mice required increased lengths of time to learn the initial task and performed at chance levels after reversal learning was initiated [24]. Consistent with reduced pain responses in humans, *Syngap1*^{+/-} mice demonstrate a similar level of reduction in pain sensitivity through hot plate tests [17]. Increased risk-taking behavior has been demonstrated through a cliff avoidance and an elevated plus maze tasks where *Syngap1*^{+/-} mice

departed an elevated platform more frequently and had a greater open arm time, respectively [16], [17]. While likely not a major factor in reduced risk-taking behavior in relation to heights, Kilinc et. al. [16] mentions visual processing should be studied to determine the downstream effects it could have on behavior. Similar to the microcephaly identified in human patients, *Syngap1*^{+/-} mice have a reduction in their absolute brain volume and while some regions of the brain, such as the somatosensory cortex, had no volume reduction, many areas including V1 and higher visual areas demonstrated a reduction in volume [16].

1.7 Hypothesis for Electrophysiology in the Visual System of *Syngap1*^{+/-} Mice

When considering the altering effects of *Syngap1* haploinsufficiency on the developmental plasticity in a mouse's brain and the long-term behavioral effects resulting from these developmental changes, it is likely that these alterations to neuronal plasticity will have effects on the normal development of the visual cortex. Based on the timing of the start of the visual critical period at P21 and the early maturation of neurons around P14-P16, it is likely that the reduction in SynGAP1 expression would have no effect on the development of receptive fields as receptive fields complete development at or before P14. However, the early maturation would likely influence the development of orientation selectivity and binocular matching since both occur after the onset of early maturation. Specifically, when looking at the effects on binocular matching, a greater mismatch of orientations in binocular matching would be expected as the process driving binocular matching requires sufficient synaptic plasticity during the critical period [25]. It is also possible connections to HVAs would be affected by the early maturation of synapses as refinement of connections from V1 to HVAs typically occurs after P7 and continues until P28-P35 [5].

To develop an understanding of how the development of the visual system is affected by *Syngap1* haploinsufficiency, a series of electrophysiological and behavioral experiments were performed. Acute monocular and binocular electrophysiological probe recordings in V1 were performed in *Syngap1*^{+/-} and wild type littermate control mice to probe the effects of reduced SynGAP1 expression on retinotopy, orientation selectivity, and binocularity. To corroborate electrophysiological findings with behavioral outcomes, behavioral trials probing visual acuity of *Syngap1*^{+/-} mice were performed. Open field tests were performed to corroborate prior study demonstrations of increased activity and impulsivity while an adaptive pairwise discrimination task was used to quantify the differences in *Syngap1*^{+/-} and littermate control behavioral responses

to an angled visual stimulus. Our results indicate there are significant alterations in the visual responses, and therefore in the visual circuitry, due to early maturation of synapses in *Syngap1*^{+/-} mice.

2. METHODS

2.1 Mouse Model Information

Syngap1 heterozygous mice (B6;129-Syngap1^{tm1Rlh/J}, JAX Strain #: 008890) and littermate control mice were used for all experiments [8]. These animals were bred and housed in animal facilities at the Purdue University Weldon School of Biomedical Engineering, and were used in accordance with a protocol approved by the Purdue Animal Care and Use Committee (PACUC). Where possible mice were group housed, except after head plate surgeries where mice were single housed due to higher levels of aggression observed post-surgery in training procedures. Mice within a range of ages after P75 but before P150 were used for experiments, except for some binocular recordings where older mice were used due to colony supply constraints. For monocular electrophysiological recordings, the mouse ages ranged from P76-P145 while for binocular recordings the mouse ages ranged from P83-P242. For behavioral tests, mice began the training period between P89 and P136.

2.2 Surgeries

The two types of surgical procedures performed were approved by PACUC and performed in accordance with all PACUC policies and the protocol on file. Care was taken to ensure health of animals to reduce any pain which they might endure through the surgery and recovery process.

2.2.1 Headplate Surgeries

A modified procedure, similar to the procedure described by Juavinett et. al. [26], with a custom headplate was performed to allow for head fixation during subsequent craniotomies and electrophysiological probe recordings. The animal was weighed before general anesthesia was induced at 2.5% isoflurane (Covetrus; Cat#: 029405) using a passive scavenging anesthesia system (VetEquip; Cat#: 901806). General anesthesia was maintained throughout the procedure at 2% isoflurane with slight adjustments to compensate for fluctuations in the animal's alertness levels. Meloxicam (Covetrus; 049755) at 5-10 mg/kg was injected subcutaneously after initial induction and before the securing of the mouse's head with ear bars from a mouse stereotaxic base (Stoelting; Cat#: 51731). After head securing with ear bars, ophthalmic ointment (Covetrus;

Cat#: 048272) was applied to the eyes and the surgical site was cleaned with dilute betadine solution (Betadine; NDC: 67618-150-09) and 70% ethanol. 2% Lidocaine (Covetrus; Cat#: 002468) was injected subcutaneously at the surgical site. The scalp was incised away and the surface of the skull was cleared of connective tissues using a micro curette (FST; Cat#: 10080-10) and flushed with sterile saline (Baxter; NDC: 0338-0048-04) before being dried thoroughly. C&B Metabond (Parkell; Cat# S380) was used to attach a custom 9 mm in diameter headplate (Figure 2) to the skull. Care was taken to center this headplate over the area of the visual cortex laterally to one side of the central suture. More C&B Metabond was used to fill in the headplate ring to ensure secure attachment of the headplate to the surface of the skull. The mice were removed from anesthesia after the C&B Metabond had completed its initial curing, typically in 3-5 minutes, and were placed within a recovery chamber on a heated pad until normal activity was observed. The mice were provided a daily identical injection of Meloxicam for three days post procedure and were single housed.



Figure 2: The custom headplate and headplate holder used for craniotomies.

2.2.2 Craniotomies

A minimum of four days post headplate attachment, a craniotomy was performed to provide access to the visual cortex for same day acute electrophysiological recordings. As described prior, mice were induced for general anesthesia at 2.5% isoflurane and maintained throughout the procedure at 2% isoflurane. Meloxicam at 5-10 mg/kg was administered subcutaneously after initial induction and the mouse was head-fixed using the headplate secured to their skull and a custom headplate holder (Figure 2). V1 was accurately located using stereotaxic coordinates at 2.5 -3 mm lateral of bregma and 3 mm posterior of bregma. This location was marked on the cured C&B Metabond using a permanent marker. Using a dental drill and liberal application of sterile artificial cerebrospinal fluid (ACSF) to the headplate well, a ring with a diameter of 1-1.5 mm was drilled around the marked location and through the cured C&B Metabond and skull. Once the

interior section of C&B Metabond and skull was loose, it was lifted away from the brain and removed. The headplate and exposed brain were repeatedly flushed with ACSF to wash away any minor bleeding and remaining debris from the craniotomy. During this flushing period, the brain was inspected for major damage and severe bleeding to ensure the mouse would be viable for the acute electrophysiological recording to follow. Once minor bleeds from the surgery and skull removal had self-clotted, the ACSF was removed from the headplate and Qwik-Sil (WPI; Cat#: QWIK-SIL), a low toxicity silicone adhesive, was applied to the exposed brain and headplate well. Qwik-Sil was used to ensure the brain was sealed away from the outside environment until electrophysiological recordings were ready to commence. After the Qwik-Sil had cured, typically in 1-3 minutes, the mouse was removed from anesthesia and allowed to recover in the recovery chamber described above. Throughout this time, the mouse was observed for signs of distress and bleeding from the brain below the Qwik-Sil covering.

2.3 Electrophysiological System and Head Fixed Recordings

2.3.1 Ephys System Description

Mice were head-fixed with the custom headplate holder used for the craniotomy procedure and were allowed to run freely on a modified version of the KineMouse wheel or a floating Styrofoam ball [27]. Using the New Scale Multi-Probe Micromanipulator (MPM) System for electrode manipulation, Cambridge Neurotech H3 Neural Probes or the open source 128AxN Sharp Masmanidis lab probes were used to obtain electrophysiological recordings (Figure 3) [28]. Electrodes were cleaned between procedures by soaking for 10 minutes in Tergazyme (Alconox; Cat#: 1304-1) before being flushed with distilled water. Additionally, the 128AxN Sharp electrodes were electroplated using an Intan RHD Electroplating board and Silfco gold solution (Sifco Acs; Cat#: 5355) to electroplate sites with gold down to 200 k Ω . All electrophysiological data was recorded using an Intan RHD USB Interface Board with a sampling rate of 20,000 Hz and the now legacy RHD USB Interface board recording software provided by Intan. A three-screen setup, described more in depth in the visual stimulation section, presented stimuli to the mice and stimuli timing was synchronized with the RHD USB Interface board using an Arduino Leonardo (Arduino; Cat#: 8058333491141). Additional moveable shutters utilizing a servo motor (Sparkfun; 9g A0090) were positioned in front of the mouse's eyes during the binocular recording

sessions to selectively occlude the mouse’s vision. The primary Arduino Leonardo board mentioned above and a second Arduino Leonardo controlled these shutters. During the binocular recording experiments with the KineMouse wheel, a rotary encoder (US Digital; H5-360-NE-S) recorded the running movements of the mouse throughout the experiment.

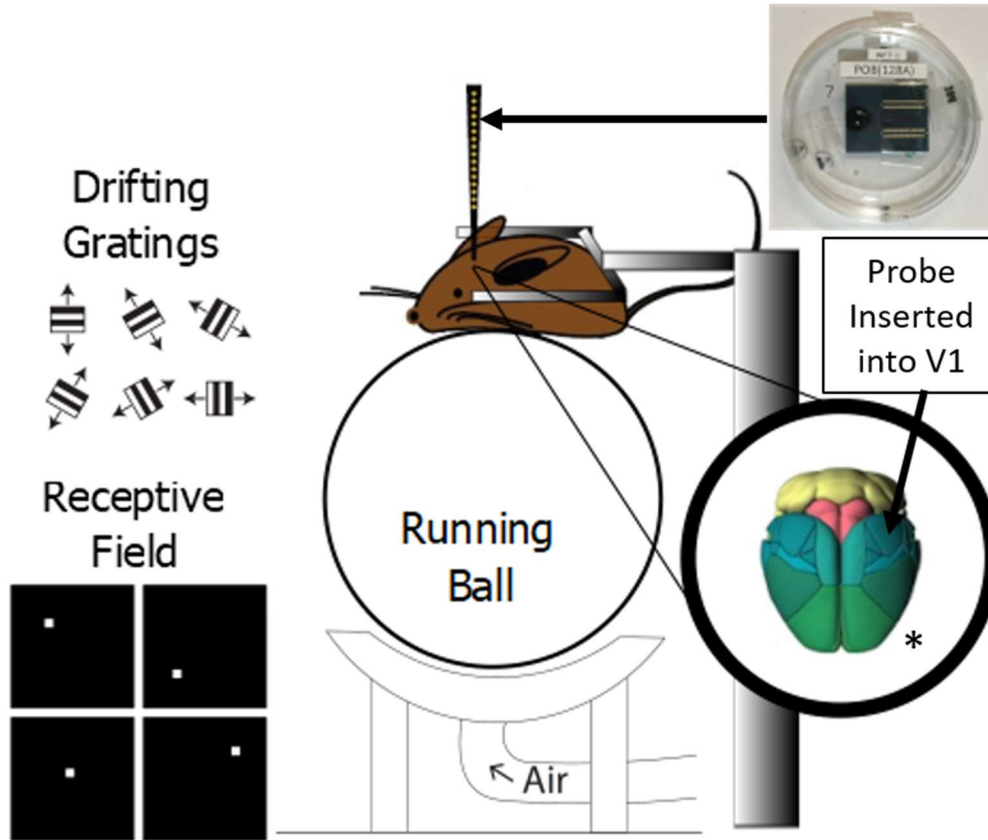


Figure 3: Acute electrophysiological recording setup. The mouse is headplated with an acute recording probe inserted into V1 and allowed to run freely on either a KineMouse wheel or styrofoam running ball. Visual stimuli on screens are placed in the visual field of the mouse during the experiment. Not shown are the Intan recording board, binocular shutters, and peripheral support equipment. *This brain image was generated from the Allen Mouse Brain Connectivity Atlas using the 3D brain explorer [29], [30]

2.3.2 Head Fixed Recording Setup and Procedure

After completing a 1-hour recovery period post craniotomy completion, the mouse was then placed on the KineMouse wheel or floating Styrofoam ball and was head-fixed to the custom headplate holder. The Qwik-Sil was removed and sterile ACSF was immediately used to fill the headplate well to protect the skull and exposed brain from the exterior environment. Using a

microscope, the brain was inspected for bleeding or any abnormal reaction to the craniotomy. A silver wire grounding electrode, used to ground the probe after implantation, was then attached to the side of the headplate and the uninsulated end was lowered into the ACSF in the headplate well away from the craniotomy. The MPM arm was maneuvered into a location which allowed for insertion in the craniotomy and the selected probe, either an H3 or 128AxN Sharp, was attached to the MPM arm. The Intan RHD USB interface board and the ground wire were attached to their respective ports on the probe. Connection tests were performed to ensure the probe was being correctly detected by the Intan recording software. Coarse adjustments of the MPM system were performed to maneuver the top of the probe just under the surface of the ACSF in the headplate well. Final adjustments were performed utilizing the MPM control system until the probe was located close to the brain's surface ($\sim 10\text{-}50\ \mu\text{m}$) over the targeted area of V1. To ensure fluctuations in the brain's motion did not snag the shank(s) during agarose preparation, the probe was moved upwards by $\sim 100\ \mu\text{m}$. 2.5% agarose, prepared prior to the procedure, was reheated and remixed in a microwave. Once the agarose was warm to the touch, the ACSF was wicked away from the headplate well and the agarose was quickly used to fill the headplate well. Immediately after application, the shank(s) were quickly forced through the surface of the brain using the coarse control ($\sim 100\ \mu\text{m}/\text{pulse}$) on the MPM system until the shanks had been observed to break thorough the brain's surface. The shanks were then slowly inserted the rest of the way over $1000\ \mu\text{m}$ at a rate of $50\ \mu\text{m}/\text{s}$. After the shank was fully inserted, the mouse was allowed to rest freely on the wheel for a minimum of 30 minutes to reduce electrode drift and any swelling due to acute trauma from the shank insertion. During this period, the visual system was moved into position and connected to the recording system. Additionally, in the binocular experiment, the shutters to selectively occlude the eyes were placed where they could block the mouse's field of view for each eye. Immediately before initiation of the visual stimulation procedure, all lights in the room were shut off to ensure the only stimulus would be from the experimental setup.

2.4 Visual Stimulation

Visual stimuli were presented to the mice using a vertically oriented three-screen setup (Dell; UltraSharp UP2716D) which covered a visual area of ~ 168 visual degrees. Stimuli were developed and presented using PsychoPy version 2020.2.10 [31]. This codebase was integrated with the Arduino Leonardos described above to allow for synchronization of stimuli presentations

and binocular recording shutter movements with electrophysiological recordings from the neural probe.

2.4.1 Monocular

Monocular stimuli were presented as a drifting grating stimulus, and a receptive field stimulus. For the drifting grating stimulus (Figure 4), the gratings were presented in a set of orientations from 0° - 330° in 30° increments and at spatial frequencies of 0.01, 0.02, 0.04, 0.08, 0.16, and 0.32 cycles/ $^{\circ}$ (cpd) [32]. The phase of these stimuli was held at 0.0167 Hz and the stimuli were presented as white on a grey background. The drifting grating stimulus was presented in a set of 20 repetitions for 30 frames (0.5 s) of stimulation time and with 30 frames (0.5 s) of blank grey screen time. The receptive field stimulus (Figure 4) was an 8x8 visual degree white square presented on a black background which was randomly placed at 4 visual degree increments across the visual field. The stimulus was presented for 20 repetitions for 6 frames (0.1 s) of stimulation time with no blank screen time.

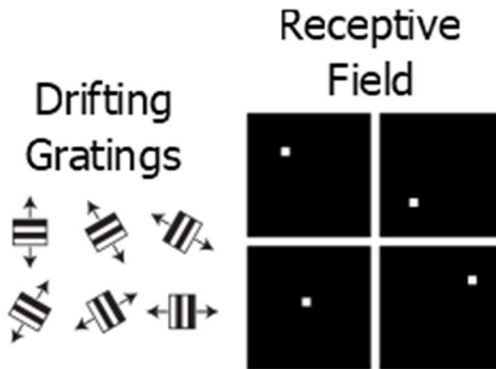


Figure 4: Examples of drifting grating and receptive field stimuli.

2.4.2 Binocular

Binocular stimuli were presented in an identical manner as for the monocular stimuli except for a few minor changes. Shutters were developed to unilaterally occlude one eye from the stimulus presentation. For both the drifting grating and receptive field stimuli, the shutters were pseudorandomly moved to always cover an eye. For the drifting grating stimuli, gratings were presented with the same orientations, spatial frequencies, and phase. Twenty repetitions were presented for each eye and the stimulation time was kept at 30 frames (0.5 s) while the blank grey

screen time was adjusted to 45 frames (0.75 s) to allow for shutter movement. For the receptive field stimulus, the sizing, location, and stimulation time remained the same, but the number of repetitions was dropped to 10 per eye. Additionally, a black screen blank screen time of 10 frames (0.17 s) was added between stimulus presentations to ensure the shutters had movement time between each stimulus.

2.5 Behavioral Experiments

2.5.1 Citric Acid Water Conditioning

Instead of water or food restriction, motivation to conduct behavioral tasks was provided by the addition of citric acid to the ad-lib water supply of the mice [33], [34]. Three days prior to the initiation of habituation in the task schedule, the mouse ad-lib water supply was switched over to water with 2% citric acid content by weight. The mouse food supply remained the same with ad-lib access. Throughout pretraining and the adaptive pairwise visual discrimination (APD) task, the concentration of citric acid in the water supply was adjusted between 0.5-2% to ensure the mice did not drop below 80% of their base weight [35].

2.5.2 Behavioral Experiment Setup and Equipment

Standardized Bussey-Saksida Mouse touch screen chambers (Campden Instruments; Cat# 80604A/614A) were the environment used to test the behavioral response to changes in the mice's visual acuity. Mice were trained in a standardized pairwise discrimination learning paradigm before being placed on the APD task [36]. Nesquik rewards were provided in ~5 μ L pulses throughout experimental pretraining and the APD task, except where explicitly noted otherwise.

2.5.3 Behavioral Experiment Pretraining

After completion of the citric acid water conditioning phase, mice began the standardized Pairwise Discrimination pretraining portion of the behavioral experiment [36]. See Table 1 for a detailed outline of the pretraining steps including reward, trial length, and advancement specifications. In general, this pretraining was intended to teach the basics of important tasks

required for the APD task such as task initiation, image selection through touch screen selection, and punishment on incorrect image selection.

Table 1: Pretraining and APD Task Regimen Outline

Experiment Stage	Description	Reward Volume	Trial Time	Success Criterion
Citric Acid Water Restriction	Mice were placed on an ad-lib, 2% citric acid (CA) spiked water supply 3 days prior to habituation. The water supply was adjusted as needed between 0.5% -2% CA content to maintain mice above 80% of their base weight.	N/A	N/A	N/A
Habituation	Mice were placed into behavioral chambers with a preplaced reward in the feeder tray and allowed to roam the chamber.	150 μ L	15 min	2 days of habituation
Initial Touch Training (ITT)	A single image was displayed pseudorandomly on one side of the screen (Left or Right). After a delay, the image was removed and the reward was provided at the feeder tray.	\sim 5 μ L/trial	60 min	30 trials
Must Touch Stimuli (MTS)	A single image was displayed pseudorandomly. After the mouse successfully touched the image, the image was removed and the reward was provided at the feeder tray.	\sim 5 μ L/trial	60 min	30 trials/day for 3 consecutive days
Must Initiate (MI)	The mouse was required to initiate the MTS task described above by first nose poking the feeder tray.	\sim 5 μ L/trial	60 min	30 trials/day for 3 consecutive days
Punish Incorrect (PI)	The MI task was performed as described above, but if the incorrect side – the one not containing the image – was selected, then a timeout was applied as punishment. After the punishment period, the mouse was required to perform a correction trial to reduce the development of stimulus side bias [37].	\sim 5 μ L/trial	60 min	23/30 trials/day (80% correct, does not include correction trials) for 3 consecutive days
APD Training Day	The APD task was run to familiarize the mouse with the stimuli presented.	\sim 5 μ L/trial	60 min	30 trials
APD Task	The mouse had to nose poke the feeder tray to initiate the trial where two images were presented pseudorandomly. When the mouse nose poked the correct image (90° angle). the reward was provided at the feeder tray. If the incorrect image was selected, the mouse entered a punishment period with subsequent correction trials. The incorrect image had an angle between 0° and 87.5° and was incremented by 2.5° throughout the experiment. When the trial set criterion was met, the incorrect image angle was incremented upwards by 2.5° and when the criterion was not met, the incorrect image angle was incremented downwards by 2.5°. At the beginning of the daily set of 60 trials, the image angle was incremented downwards by 5°	\sim 5 μ L/trial	60 min	8/10 trials in a 10 trial set (80% correct, does not include correction trials); 60 total trials per day

2.5.4 Adaptive Pairwise Visual Discrimination (APD) Task

An adaptive version of the visual discrimination task described in Horner et. al. [36] allowed for steady and controlled incrementation of the visual angle of the incorrect stimulus towards the 90° correct stimulus (Figure 5). A detailed outline of the incrementation control and criteria to alter the incorrect stimulus angle is located in Table 1. The initial day the mice were on the task was treated as a training day to allow the mice to learn the increasing angle aspect of the task and that the correct stimulus was at 90° . The following day, the mice were placed on the task and allowed to progress until long term leveling out of training progress for 5 days had been perceived population wide.

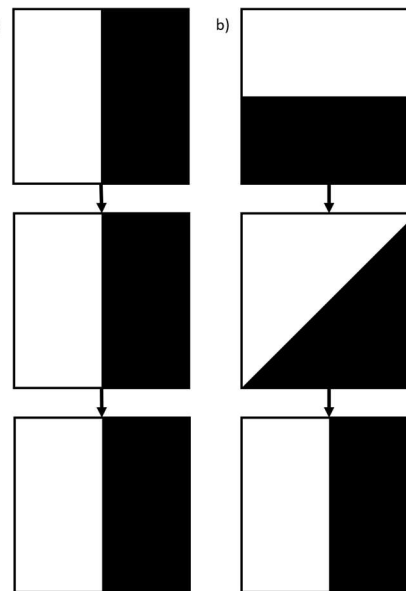


Figure 5: Angle incrementation for the APD task. a) Correct stimulus always remains at 90° . b) Incorrect stimulus begins at 0° and increments by 2.5° towards 90°

2.5.5 Mouse Activity Boxes

General activity levels were determined through an open field system (Omnitech Electronics; SuperFlex Open Field). Two days post completion of the APD task when mice were back on ad-lib water without citric acid, mice were placed into the system for 15 minutes and allowed to roam at will around the open field area. No reward was provided for this task.

2.6 Electrophysiological Recording Analysis

2.6.1 Electrophysiological Data Preparation Process

Data from the Intan USB RHD interface board was saved to a computer in the .rhd file format from the Intan recording software in either one- or five-minute increments. Utilizing a MATLAB .rhd file reader function provided by Intan and slightly altered for automation purposes, the data was parsed into a .bin format for spike sorting using Kilosort 2.5 [38]. Kilosort 2.5 is an automated spike sorting algorithm with drift correction to account for movement in the brain or electrodes during recording sessions. While this automated spike sorting greatly simplifies and

drastically expedites neuron identification, it is not flawless. Therefore, Phy was used to confirm the spike sorting performed by Kilosort 2.5. Phy provides a graphical user interface to inspect and visualize spikes which have been identified by automated spike sorting protocols [39]. All additional analysis on the spike sorted data was performed through custom MATLAB scripts.

2.6.2 Receptive Field Sizing

The neural receptive field sizes were estimated through a model-free method. The size was taken to be the spread of neural activity over the visual field, calculated in Equation (1) where x_i and y_i refer to the x and y coordinates within the visual field to which the neuron was highly responsive. “Highly responsive” was taken to be 80% of the maximum response across the entire field. Neural responses across the entire visual field were first compared to the threshold metric, and the spread was calculated for the resulting over threshold distribution of activity.

$$spread = \left(\frac{0.5}{N}\right) * sum_i(x_i - x_{mean}) + \left(\frac{0.5}{N}\right) * sum_i(y_i - y_{mean}) \quad (1)$$

2.6.3 Tuning Curve Isolation

From the spike sorted data, the recorded data specific to the tuning curve stimuli was isolated and the timing of spikes for neurons identified by the spike sorting process was identified. Neurons firing below a 0.2 Hz firing rate threshold were removed from the analysis. Tuning curves were created by summing on a per trial basis the number of spikes from each neuron within each stimulus presentation period. The average orientation response across trials for each spatial frequency was calculated to present final tuning curves.

2.6.4 Orientation Selectivity Index and Circular Variance

Two measurements demonstrated the preferred orientation response of the neurons which met the 0.2 Hz cutoff for the creation of tuning curves. The first metric, the orientation selectivity index (OSI) acts as a measure of the relative response of the neuron’s preferred orientation compared to the orthogonal orientation. This works as a measure of the neurons tuning to that preferred orientation. OSI was calculated using Equation (2), where R_{pref} is the peak response or the number of spikes within the stimulus period for the preferred orientation and R_{ortho} is the orthogonal response [32].

$$\frac{R_{pref} - R_{ortho}}{R_{pref} + R_{ortho}} \quad (2)$$

A higher OSI value (Figure 6) closer to 1 indicates the neuron has greater selectivity, while a lower response closer to 0 indicates the neuron has a lower selectivity.

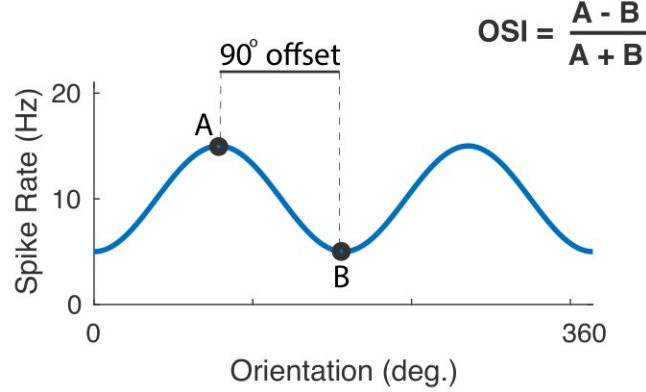


Figure 6: Example of OSI calculations in reference to a sinusoidal example tuning curve. The second metric is circular variance which looks at the average of the response of the neuron to the two directions of motion for each orientation. While circular variance can be calculated using Equation (3), and the corresponding calculation for R shown in Equation (4), it can be more easily approximated by fitting the tuned response to the cosine function presented in Equation (5), where A is the mean response of the cell across all orientations sampled, B is the amplitude of the response at the preferred orientation, and θ_{pref} is the orientation angle which is preferred by the cell [40].

$$V = 1 - |R| \quad (3)$$

$$R = \frac{\sum_k r_k e^{i2\theta_k}}{\sum_k r_k} \quad (4)$$

$$R(\theta) = A + B \cos(2(\theta - \theta_{pref})) \quad (5)$$

From this cosine function, the circular variance can be calculated using Equation (6).

$$V = 1 - \frac{B}{2A} \quad (6)$$

Using circular variance as a metric, highly selective cells will have a circular variance close to 0 (Figure 7) as there will be less spread in the tuning of the neuron, while less selective cells will have a circular variance close to 1 as there will be a greater spread in the tuning of the neurons.

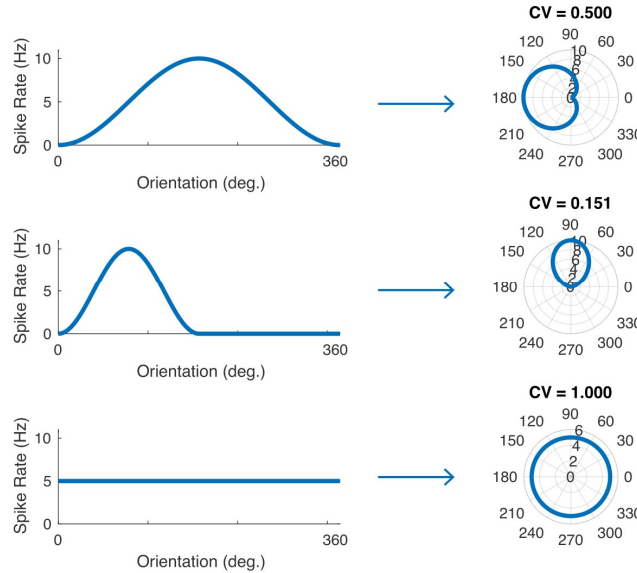


Figure 7: Example of how CV demonstrates neuronal tuning in reference to example tuning curves

2.6.5 Neuronal Firing Rate

The firing rate was first calculated as shown in Equation (7) as a population firing rate and the results were compared to the 0.2 Hz firing rate threshold to remove slow firing neurons from the tuning curve and receptive field analyses. After the tuning curve analysis was performed and the tuned neurons were isolated, the firing rate for tuned and untuned neurons was calculated separately using Equation (7).

$$firing\ rate\ \left(\frac{spikes}{s}\right) = \frac{total\ number\ of\ spikes}{total\ number\ of\ samples} * sampling\ rate \quad (7)$$

2.6.6 Ocular Dominance Index

To determine the measure of how dominant one eye's response is compared to the other eye, the ocular dominance index was calculated as a measure of binocularity. Equation (8) was used [32] where 'C' is the maximum response of the contralateral eye and 'I' is the maximum response of the ipsilateral eye.

$$ODI = \frac{C - I}{C + I} \quad (8)$$

The ODI serves as the ratio of the maximum responses of both eyes with an ODI closer to zero indicating better match in orientations between the eyes. Additionally, the difference in preferred direction was calculated using Equation (9) where PD_C is the preferred direction for the contralateral eye and PD_I is the preferred direction for the ipsilateral eye.

$$\Delta PD = PD_C - PD_I \quad (9)$$

2.6.7 d-Prime Analysis

To understand how the population of neurons in the visual cortex together represent a visual stimulus in *Syngap1*^{+/-} mice compared to wild type mice, we used \mathbf{d}' , a metric which is commonly used to measure discriminability between two signals or between a signal and noise [41], [42]. D-prime is calculated as shown in Equation (10), where d' is the difference between the means of two distributions (μ_1 and μ_2) normalized by the squared difference between the variance of the two distributions (σ_1^2 and σ_2^2) [41], [42].

$$d' = \frac{\mu_1 - \mu_2}{\sqrt{\sigma_1^2 - \sigma_2^2}} \quad (10)$$

To measure discriminability of population-level responses to distinct visual stimuli, the dimensionality of the neural dataset was reduced using Principal Component analysis (PCA). Only the first two principal components were kept which accounted for 51.4% of the variance in neural responses. With this process, a ~ 100 length vector of responses per trial was reduced to a 2 x 1 vector in principal component (PC) space, where x_i denotes the single-trial representation in 2-dimensional PC space for trial i . For each pair of visual stimuli (e.g., gratings moving in directions 0° and 45°), all trials for stimuli in each of these two movement directions were selected and thereby separated into two corresponding groups. Taking the difference between the two means yielded a vector, \vec{v} , between the average of the two population-level responses. The individual trials were then projected onto \vec{v} by taking the dot product, $p_i = \vec{x}_i \cdot \vec{v}$, and d' as shown in Equation (10) was calculated from the means and variance of the set of trials associated with each stimulus direction.

As demonstrated in Figure 8, a higher d' value indicates the signals are more different, and therefore there is a greater ability to discriminate between the two angles being presented. Likewise, when the d' value is closer to zero, there is less difference between the signals, and therefore they are harder to discriminate from each other.

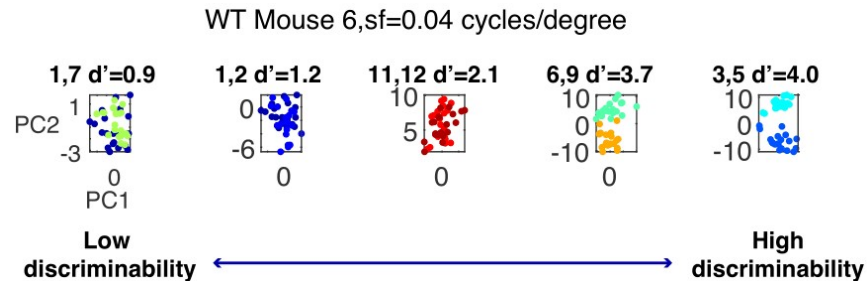


Figure 8: Examples of discrimination ability between two angles for a neuron with high and low d' values.

2.7 Behavioral Data Analysis

2.7.1 Open Field Activity Analysis

Mouse activity data from the SuperFlex Open Field system was analyzed utilizing the built in Fusion protocol development, implementation, and analysis software. This software tracks the movement of the animal in the open field system and was used to automatically generate heatmaps for the population of mice split by genotype. Additionally, movement timing and speed data was gathered for statistical tests run in MATLAB.

2.7.2 APD Data Analysis

After isolating the data from the Bussey-Saksida Mouse touch screen chambers using ABETII, the dataset was analyzed in MATLAB. From the overall dataset, the latency from trial initiation to correct image touch was isolated. These latencies were averaged for each trial day across the genotype population and compared for statistical significance across genotypes using a Wilcoxon rank sum test. Additionally, the final angle reached in each training day was isolated from the data as a metric of learning and discrimination threshold. The training progress was graphed to indicate where the leveling out of learning progress for the mice began. The final angle from the last five

days of training were gathered and a Wilcoxon rank sum test was performed to isolate differences in the discrimination threshold of the two genotype groups.

3. RESULTS

3.1 Receptive field spread remained similar among wild type and *Syngap1*^{+/-} neurons

Both *Syngap1*^{+/-} and wild type mice expressed selective receptive fields alongside some non-selective receptive fields as seen in Figure 9. The spread of the receptive fields was analyzed as described in the methods section. To remove low firing (<0.2 Hz) and nonresponsive neurons from the analysis, only the receptive fields of tuned neurons were analyzed. This Wilcoxon rank sum analysis determine there was no statistical difference in the size of the receptive fields of either *Syngap1*^{+/-} or wild type mice (Figure 9).

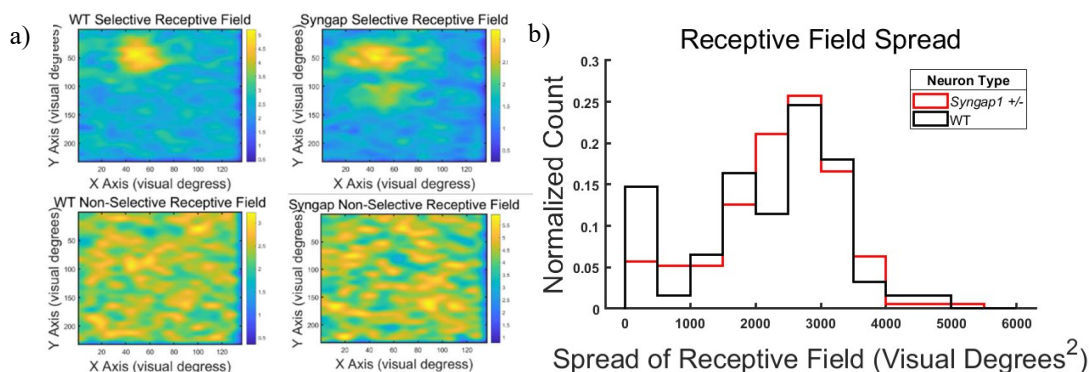


Figure 9: a) Examples of receptive and non-receptive fields in *Syngap1*^{+/-} and wild type mice. b) Spread of receptive field selectivity ($p = 0.2894$).

3.2 Orientation selectivity was reduced in *Syngap1*^{+/-} mice

Both *Syngap1*^{+/-} mice and wild type littermate controls demonstrated strong tuning curves in response to drifting grating stimuli (Figure 10). The strongest tuning curve responses appeared at spatial frequencies of 0.04 and 0.08 as indicated by Niell et. al. [32] so tuning responses were analyzed at the spatial frequency of 0.04. For the orientation selectivity index, *Syngap1*^{+/-} mice had an average lower OSI value (mean OSI = 0.317) compared to wild type controls (mean OSI = 0.374), indicating wider and less selective tuning to neural responses. For circular variance, *Syngap1*^{+/-} mice were found to have a higher average CV value (mean CV = 0.902) compared to wild type controls (mean CV = 0.885) indicating similarly wider and less selective tuning responses like the OSI metric. Both metrics were found to have statistically significant differences in OSI an CV indicating that neurons in *Syngap1*^{+/-} mice do have wider tuning.

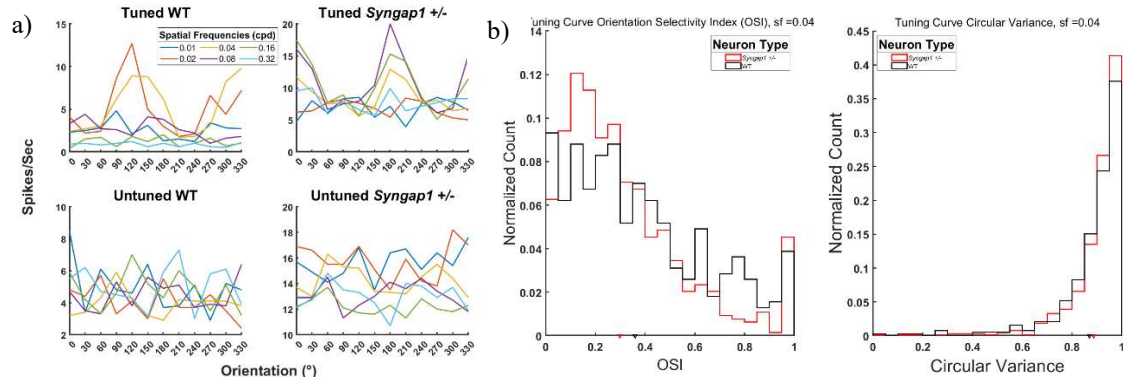


Figure 10: a) Examples of specific and non-specific tuning curves from wild type littermate controls and *Syngap1* +/- mice. b) Tuning curve OSI ($p = 0.0013$) and CV ($p = 0.0287$) histograms.

3.3 Tuned *Syngap1* +/- neurons demonstrate a depressed firing rate

The firing rate of the neurons recorded during the monocular recordings sessions was analyzed to identify if *Syngap1* heterozygosity had perturbed the firing rate of neurons in V1. First, the overall firing rates of all neurons over the 0.2 Hz threshold were calculated (Figure 11) and after testing, no significant difference was found. When splitting the neurons by tuned and untuned neurons, there was a statistical difference in the firing rates of the tuned neurons. Specifically, the wild type tuned neurons had a higher firing rate with a mean of 4.28 Hz compared to the *Syngap1* +/- tuned neurons which had a mean firing rate of 1.88 Hz.

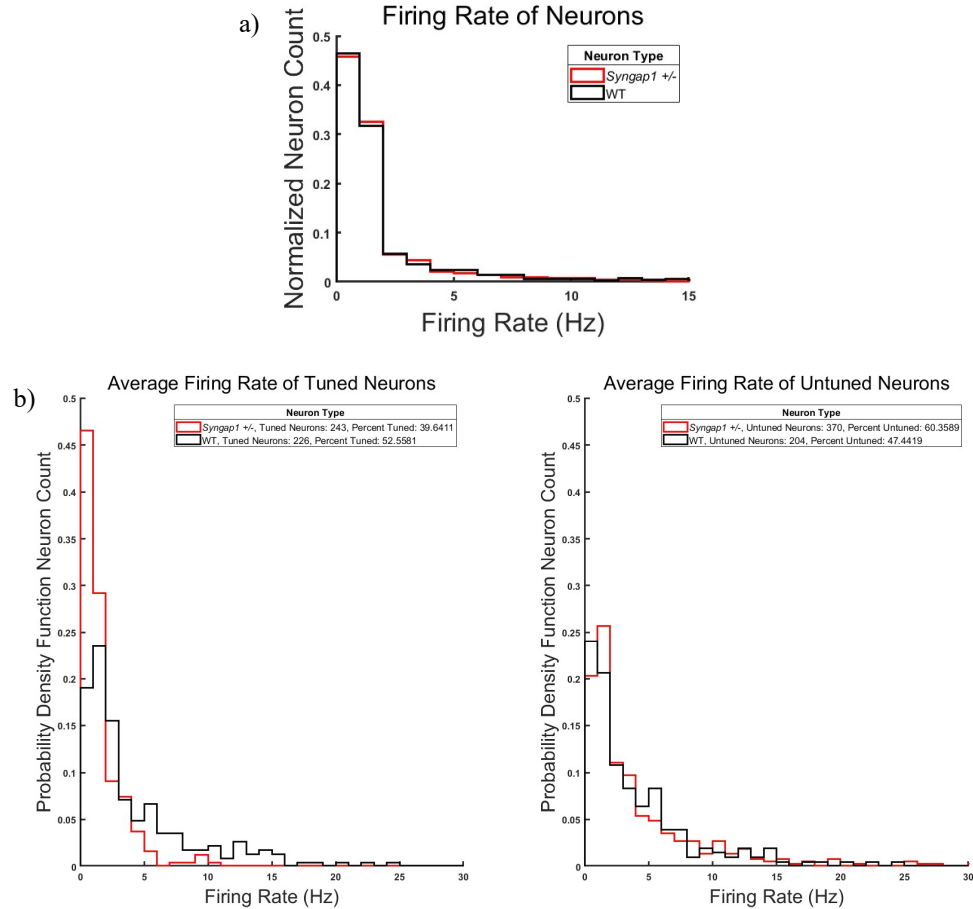


Figure 11: Histograms of firing rates for monocular recording neurons. a) Overall firing rate of all neurons over the 0.2 Hz threshold ($p = 0.5166$). b) Firing rate of tuned and untuned neurons (Tuned: $p = 8.2081e-12$, Untuned: $p = 0.9165$)

3.4 No significant differences in binocular matching detected through the ODI

The ocular dominance index (ODI) for binocular matching was calculated as the main indicator of orientation matching between the ipsilateral and contralateral eyes. As can be seen in Figure 12, the ODIs for both *Syngap1*^{+/-} and wild type controls were distributed in a similar manner. In statistical testing, no difference was found in the ODIs for either group. Additionally, the differences in preferred direction for each neuron were compared and after a Wilcoxon rank sum test, no statistical difference was identified. These results indicate that there appears to be no significant difference in the ability of *Syngap1*^{+/-} to have binocularly matched neurons.

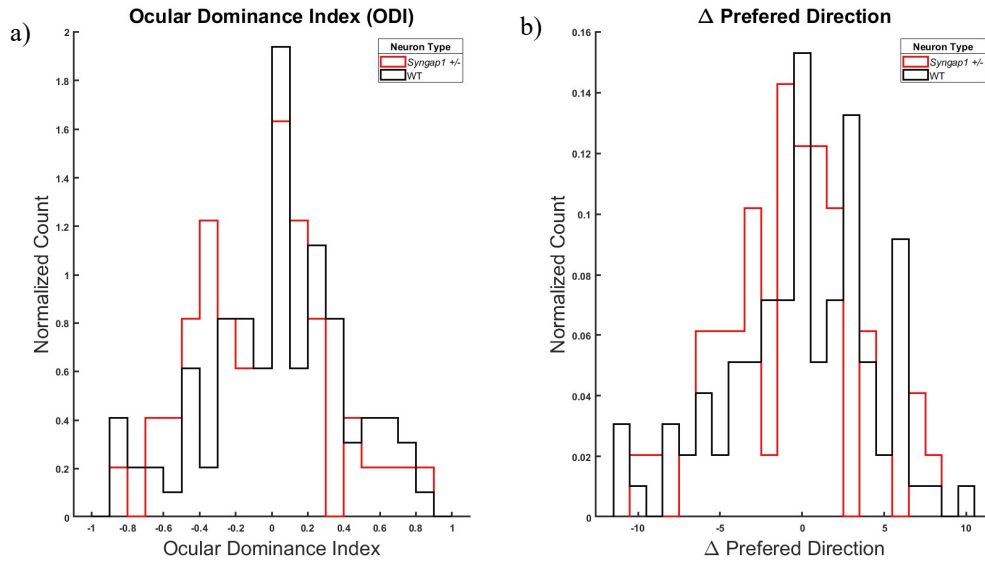


Figure 12: Histograms demonstrating binocular matching responses of neurons. a) ODI Response ($p = 0.1544$). b) Difference in preferred direction ($p = 0.1864$)

3.5 Population level analysis indicates differences in neural responses

To probe population level responses, the d' values of neurons was analyzed as described before. As is demonstrated in Figure 13, there was a significant difference in the d' values of *Syngap1*^{+/-} and wild type mice. Specifically, *Syngap1*^{+/-} mice had significantly lower d' values than the wild type mice. This indicates a population level difference in the ability of specific neurons to discriminate between two different angles.

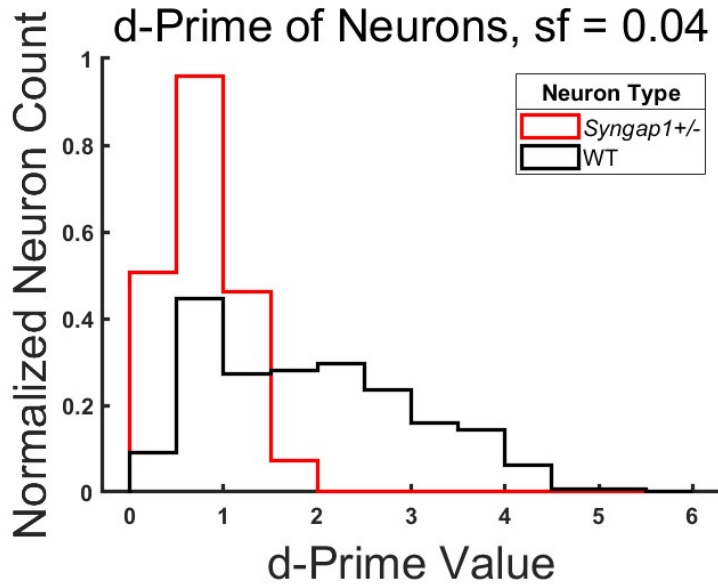


Figure 13: d' analysis of neurons. $p = 7.6337 \times 10^{-50}$

3.6 *Syngap1*^{+/-} mice exhibit increased hyperactivity and impulsivity

Syngap1^{+/-} mice exhibited hyperactive behaviors in the open field activity analysis from the SuperFlex Open Field system. As can be seen in the heat maps of Figure 14, the *Syngap1*^{+/-} mice moved throughout the cage much more widely than the littermate control mice. While statistical differences, calculated by Wilcoxon rank sum tests, were not detected in the fraction of time spent moving, number of discrete movements, or peak velocities, the *Syngap1*^{+/-} mice had a consistently higher movement velocity and traveled farther in each period of movement than the wild type mice did. Overall, this indicates greater consistent movement from the *Syngap1*^{+/-} mice. Additionally, during the APD task the mice demonstrated a decreased response latency from trial initiation to correct image selection compared to the wild type mice (Figure 15). This indicates an increase in the impulsivity of the *Syngap1*^{+/-} compared to the wild type mice.

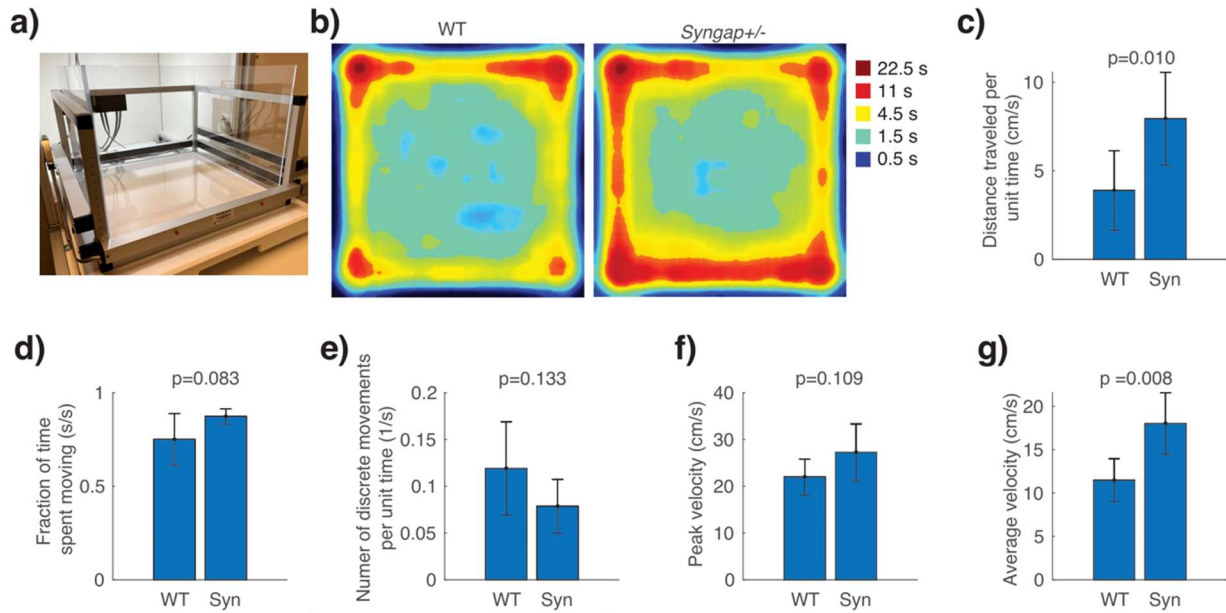


Figure 14: Results from the open field activity of *Syngap1*^{+/-} and littermate controls. a) SuperFlex Open Field System. b) Heatmap of movement around cage for mice separated by, and average across the mouse genotype. c-g) Mobility metrics compared between the two genotypes utilizing a Wilcoxon rank sum test.

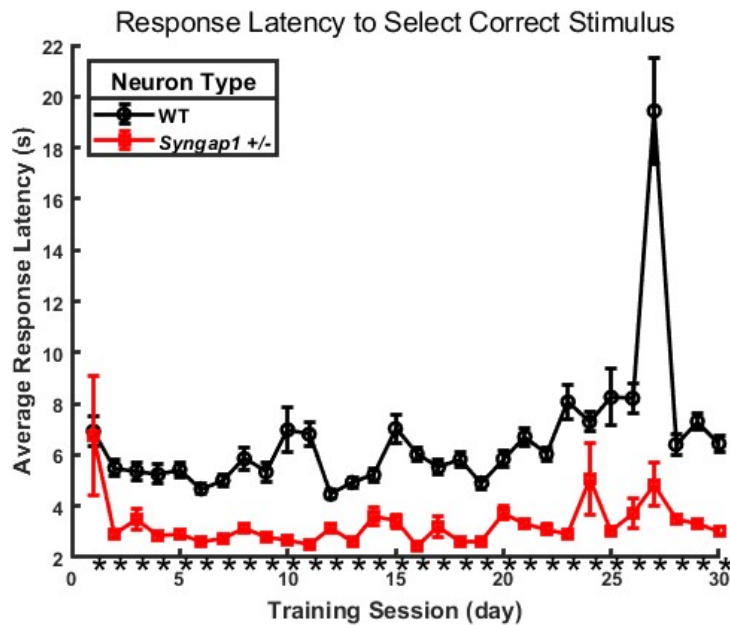


Figure 15: Average latency response to select correct stimulus after initiation of the trial. The stars indicate training sessions where a Wilcoxon rank sum test found significance of $p < 0.05$.

3.7 *Syngap1*^{+/-} mice had difficulty discriminating finer angles

After performing the pretraining paradigm and the initial task learning day, the behavioral mice were transitioned to the APD task. While some mice were able to quickly learn the task, some mice took longer to learn the discrimination portion of the task and only began to increment their angles upwards around training day 10 (Figure 16). There were no differences across animal genotype for how quickly the task was learned as both wild type and *Syngap1*^{+/-} mice had difficulty learning the task. As the mice proceeded through the task, their progress began to level out and around day 25 they had leveled out sufficiently to test for differences in discrimination threshold. Looking at the last 5 days of the task when the mice had leveled out, a Wilcoxon rank sum test (Figure 16) of the final reached angle each day found that *Syngap1*^{+/-} mice had a statistically higher discrimination threshold at an average of 23° compared to their littermate controls with an average angle of 17°. This indicates that the *Syngap1*^{+/-} mice had a greater difficulty in discriminating between the 90° correct angle and the incrementally increasing incorrect angle.

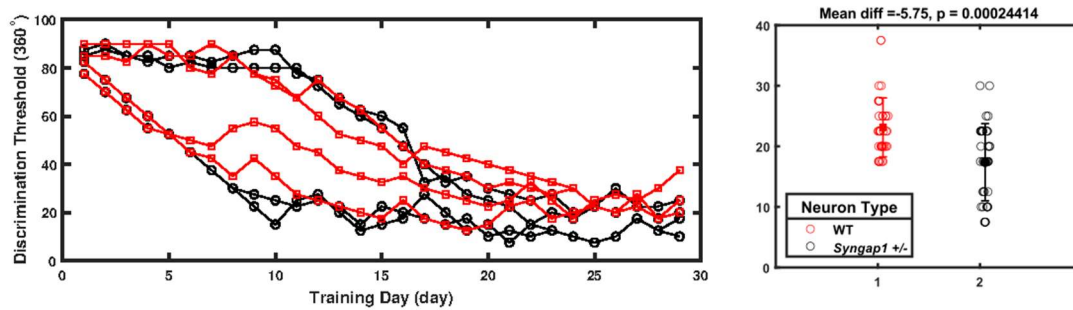


Figure 16: APD task demonstration of long-term task learning and statistical differences in the discrimination threshold of *Syngap1*^{+/-} mice and wild type controls.

4. DISCUSSION AND CONCLUSIONS

These results demonstrate the early maturation of synapses due to a lack of SynGAP1 influences the development and function of the visual system in *Syngap1*^{+/-} mice. Based on the time frame for early synapse maturation around P14-P16, minimal changes were hypothesized to be seen in retinotopy due to its earlier development and larger changes were hypothesized to be identified in orientation selectivity and binocularity. As expected, no major changes in retinotopy were detected through the analysis of receptive fields. Both *Syngap1*^{+/-} and wild type mice exhibited normal receptive fields and there was no significant difference in the spread of receptive fields. This indicates that SynGAP1 likely has no major effect in the innate development of these receptive fields as their development is not driven by visual experience.

As eye opening occurs and SynGAP1 concentrations shift into the synapse, orientation selectivity begins to develop. While orientation selectivity is an innate process, it is reinforced by experience which requires LTP to strengthen synapses, and therefore SynGAP1 expression for optimal refinement [2]. Analysis of the orientation selectivity of neurons through tuning curves demonstrated a reduced tuning specificity in *Syngap1*^{+/-} mice compared to their littermate controls. This alteration in tuning specificity was analyzed on a neuronal population level through a *d'* analysis which demonstrated a reduced ability to discriminate angular stimuli information. This reduced specificity would correspond to the reduced refinement effects from a reduction in optimal LTP strengthening of synapses from visual stimuli.

Binocularity develops during the visual critical period from P21-P35 and is defined by behavioral dependence to allow for optimal matching of orientation selectivity from both eyes. As a reduction in SynGAP1 reduces the plastic response of neurons, it would be expected that binocularity in *Syngap1*^{+/-} mice would also be altered in some way. However, no statistically significant difference in ODI or the difference in preferred directions of neurons in binocular recordings was discovered. While the statistics are valid, it is important to note that the population size for the binocular experiment was small (49 WT neurons, 98 *Syngap1*^{+/-} neurons) and used older mice. It is likely more minute aberrations in binocularity could be detected with a larger population size.

As discussed in multiple sources, *Syngap1*^{+/-} mice express hyperactivity and impulse control issues [17], [24]. The open field tests and latency to respond to the APD task from initiation,

corroborate that *Syngap1*^{+/-} mice are hyperactive and impulsive. Additionally, while some studies in humans described aggressive behaviors, no studies on *Syngap1*^{+/-} animals have provided a distinct understanding of aggression in these mice [7], [17]. In some instances, during the group housing of *Syngap1*^{+/-} mice and particularly after head plate surgeries, aggressive behaviors consisting of intense barbering and associated flesh wounds were observed by animal care and experimental staff. While these empirical observations could not be studied through a controlled behavioral study, care was taken to reduce aggressive behavioral interactions among mice by single housing after surgery.

Correlating neural activity with behavioral responses is critical for developing a full understanding of downstream effects of alterations to neural circuit function. The APD task isolated the visual discrimination differences of *Syngap1*^{+/-} mice and determined if neural effects from V1 were in part responsible for behavioral changes. The results of this task demonstrated that the mice were able to learn a behavioral task in an effective manner and discriminate an angled stimulus up until their innate visual discrimination threshold. This task found a significant increase in the discrimination threshold of *Syngap1*^{+/-} mice, indicating that it is likely more difficult for them to discriminate between fine angle differences. Considering the reduced orientation selectivity demonstrated from monocular recordings, these behavioral effects could be influenced by alterations in V1. It is also important to consider that V1 innervates HVAs which may play a critical role in providing information for decision making to other brain regions. Additionally, while efforts were taken to remove any effect of impulsiveness on the APD task, the impulsiveness and hyperactivity demonstrated by *Syngap1*^{+/-} mice should be considered as a confounding factor.

It is evident that *Syngap1* heterozygosity affects the development and function of V1, and likely HVAs to some extent. However, the mechanics controlling these developmental changes, and the resulting aberrations in visual processing are still not well understood. To provide a greater understanding of the neural differences, more binocular recordings should be performed, alongside recordings in higher visual areas. The greater number of binocular recordings should be performed to ensure that significance in the results is reached as a power analysis revealed the number of neurons analyzed was not enough to be statistically significant. The targeting of higher visual areas is critical because their innervation and refinement from V1 spans from P7-P35, before the alteration in SynGAP1 levels and at the end of the critical period. Isolating neural responses in this area can demonstrate how aberrations in V1 processing affect higher level visual processing.

Additionally, performing recordings within the developmental timeframe of visual development would provide information on specific differences in the development of visual processing characteristics. For example, probing before, during, and after the development of orientation selectivity might provide information on the rate of orientation selectivity development or the level of refinement at specific developmental checkpoints.

In linking neural data with behavioral data, it is critical to reduce confounding factors in the isolation of the behavior being studied. Additional behavioral data, both to improve the power of the behavioral experiment, and to allow for refinement of the visual discrimination task would allow for a reduction in these confounding factors along with a more refined understanding of discrimination threshold results. Specifically, decreasing the incrementation angle change for the APD task would allow for a more refined test of visual acuity while improving the pretraining would help to reduce impulse related issues with the task. By deepening the understanding of visual circuit development in *Syngap1*^{+/-} mice, a greater understanding of the functional roles SynGAP1 plays in neural plasticity can be elucidated.

REFERENCES

- [1] C. R. Siu and K. M. Murphy, “The development of human visual cortex and clinical implications,” *Eye and Brain*, vol. 10, p. 25, 2018, doi: 10.2147/EB.S130893.
- [2] J. S. Espinosa and M. P. Stryker, “Development and Plasticity of the Primary Visual Cortex,” *Neuron*, vol. 75, no. 2, pp. 230–249, Jul. 2012, doi: 10.1016/J.NEURON.2012.06.009.
- [3] L. Busse, “The Mouse Visual System and Visual Perception,” *Handbook of Behavioral Neuroscience*, vol. 27, pp. 53–68, Jan. 2018, doi: 10.1016/B978-0-12-812012-5.00004-5.
- [4] N. L. Rochefort, M. Narushima, C. Grienberger, N. Marandi, D. N. Hill, and A. Konnerth, “Development of direction selectivity in mouse cortical neurons,” *Neuron*, vol. 71, no. 3, pp. 425–432, Aug. 2011, doi: 10.1016/J.NEURON.2011.06.013/ATTACHMENT/F17F64E4-1321-4CA7-BC14-48540BDEEADB/MMC1.PDF.
- [5] L. L. Glickfeld and S. R. Olsen, “Higher-Order Areas of the Mouse Visual Cortex,” <https://doi-org.ezproxy.lib.purdue.edu/10.1146/annurev-vision-102016-061331>, vol. 3, pp. 251–273, Sep. 2017, doi: 10.1146/ANNUREV-VISION-102016-061331.
- [6] E. R. Kandel, J. H. Schwartz, T. M. Jessel, S. A. Siegelbaum, and A. J. Hudspeth, *Principles of Neural Science*, 5th ed. .: McGraw-Hill Companies, 2013.
- [7] T. R. Gamache, Y. Araki, and R. L. Huganir, “Twenty Years of SynGAP Research: From Synapses to Cognition,” *Journal of Neuroscience*, vol. 40, no. 8, pp. 1596–1605, Feb. 2020, doi: 10.1523/JNEUROSCI.0420-19.2020.
- [8] J. H. Kim, H. K. Lee, K. Takamiya, and R. L. Huganir, “The Role of Synaptic GTPase-Activating Protein in Neuronal Development and Synaptic Plasticity,” *Journal of Neuroscience*, vol. 23, no. 4, pp. 1119–1124, Feb. 2003, doi: 10.1523/JNEUROSCI.23-04-01119.2003.
- [9] G. Gou *et al.*, “SynGAP splice variants display heterogeneous spatio-temporal expression and subcellular distribution in the developing mammalian brain,” *Journal of Neurochemistry*, vol. 154, no. 6, pp. 618–634, Sep. 2020, doi: 10.1111/JNC.14988.

- [10] Y. Araki, M. Zeng, M. Zhang, and R. L. Huganir, “Rapid Dispersion of SynGAP from Synaptic Spines Triggers AMPA Receptor Insertion and Spine Enlargement during LTP,” *Neuron*, vol. 85, no. 1, pp. 173–189, Jan. 2015, doi: 10.1016/J.NEURON.2014.12.023/ATTACHMENT/9F9F6E26-A74B-41F9-8F42-51BE7E8C39E6/MMC2.MP4.
- [11] H. J. Carlisle, P. Manzerra, E. Marcora, and M. B. Kennedy, “SynGAP Regulates Steady-State and Activity-Dependent Phosphorylation of Cofilin,” *Journal of Neuroscience*, vol. 28, no. 50, pp. 13673–13683, Dec. 2008, doi: 10.1523/JNEUROSCI.4695-08.2008.
- [12] Y. Araki *et al.*, “Syngap isoforms differentially regulate synaptic plasticity and dendritic development,” *Elife*, vol. 9, pp. 1–28, Jun. 2020, doi: 10.7554/ELIFE.56273.
- [13] M. W. Barnett *et al.*, “Synaptic Ras GTPase Activating Protein Regulates Pattern Formation in the Trigeminal System of Mice,” *Journal of Neuroscience*, vol. 26, no. 5, pp. 1355–1365, Feb. 2006, doi: 10.1523/JNEUROSCI.3164-05.2006.
- [14] J. P. Clement *et al.*, “Pathogenic SYNGAP1 mutations impair cognitive development by disrupting maturation of dendritic spine synapses,” *Cell*, vol. 151, no. 4, pp. 709–723, Nov. 2012, doi: 10.1016/J.CELL.2012.08.045/ATTACHMENT/F4EA3537-5044-4EC9-B217-49709BDFB1EE/MMC4.MOV.
- [15] M. Aceti *et al.*, “Syngap1 haploinsufficiency damages a postnatal critical period of pyramidal cell structural maturation linked to cortical circuit assembly,” *Biological Psychiatry*, vol. 77, no. 9, pp. 805–815, May 2015, doi: 10.1016/J.BIOPSYCH.2014.08.001.
- [16] M. Kilinc *et al.*, “Species-conserved SYNGAP1 phenotypes associated with neurodevelopmental disorders,” *Molecular and Cellular Neuroscience*, vol. 91, pp. 140–150, Sep. 2018, doi: 10.1016/J.MCN.2018.03.008.
- [17] R. Nakajima *et al.*, “Comprehensive behavioral analysis of heterozygous Syngap1 knockout mice,” *Neuropsychopharmacology Reports*, vol. 39, no. 3, pp. 223–237, Sep. 2019, doi: 10.1002/NPR2.12073.
- [18] J. A. Kosmicki *et al.*, “Refining the role of de novo protein-truncating variants in neurodevelopmental disorders by using population reference samples,” *Nature Genetics* 2017 49:4, vol. 49, no. 4, pp. 504–510, Feb. 2017, doi: 10.1038/ng.3789.

- [19] D. R. M. Vlaskamp *et al.*, “SYNGAP1 encephalopathy: A distinctive generalized developmental and epileptic encephalopathy,” *Neurology*, vol. 92, no. 2, pp. E96–E107, Jan. 2019, doi: 10.1212/WNL.0000000000006729/VIDEO-2.
- [20] M. Weldon, M. Kilinc, J. Lloyd Holder, and G. Rumbaugh, “The first international conference on SYNGAP1-related brain disorders: A stakeholder meeting of families, researchers, clinicians, and regulators,” *Journal of Neurodevelopmental Disorders*, vol. 10, no. 1, pp. 1–6, Feb. 2018, doi: 10.1186/S11689-018-9225-1/FIGURES/1.
- [21] D. Prchalova, M. Havlovicova, K. Sterbova, V. Stranecky, M. Hancarova, and Z. Sedlacek, “Analysis of 31-year-old patient with SYNGAP1 gene defect points to importance of variants in broader splice regions and reveals developmental trajectory of SYNGAP1-associated phenotype: Case report,” *BMC Medical Genetics*, vol. 18, no. 1, pp. 1–7, Jun. 2017, doi: 10.1186/S12881-017-0425-4/FIGURES/2.
- [22] M. J. Parker *et al.*, “De novo, heterozygous, loss-of-function mutations in SYNGAP1 cause a syndromic form of intellectual disability,” *American Journal of Medical Genetics Part A*, vol. 167, no. 10, pp. 2231–2237, Oct. 2015, doi: 10.1002/AJMG.A.37189.
- [23] S. Chung and J. W. Son, “Visual Perception in Autism Spectrum Disorder: A Review of Neuroimaging Studies,” *Journal of the Korean Academy of Child and Adolescent Psychiatry*, vol. 31, no. 3, p. 105, Jul. 2020, doi: 10.5765/JKACAP.200018.
- [24] A. E. Horner *et al.*, “Learning and reaction times in mouse touchscreen tests are differentially impacted by mutations in genes encoding postsynaptic interacting proteins SYNGAP1, NLGN3, DLGAP1, DLGAP2 and SHANK2,” *Genes, Brain and Behavior*, vol. 20, no. 1, p. e12723, Jan. 2021, doi: 10.1111/GBB.12723.
- [25] B. S. Wang, R. Sarnaik, and J. Cang, “Critical Period Plasticity Matches Binocular Orientation Preference in the Visual Cortex,” *Neuron*, vol. 65, no. 2, pp. 246–256, Jan. 2010, doi: 10.1016/J.NEURON.2010.01.002/ATTACHMENT/C0A0410B-67B0-47C0-9DED-9896D8CB39C1/MMC1.PDF.
- [26] A. L. Juavinett, I. Nauhaus, M. E. Garrett, J. Zhuang, and E. M. Callaway, “Automated identification of mouse visual areas with intrinsic signal imaging,” *Nature Protocols 2016 12:1*, vol. 12, no. 1, pp. 32–43, Dec. 2016, doi: 10.1038/nprot.2016.158.
- [27] R. A. Warren *et al.*, “A rapid whisker-based decision underlying skilled locomotion in mice,” *Elife*, vol. 10, pp. 1–27, 2021, doi: 10.7554/ELIFE.63596.

- [28] L. Yang, K. Lee, J. Villagrancia, and S. C. Masmanidis, “Open source silicon microprobes for high throughput neural recording,” *Journal of Neural Engineering*, vol. 17, no. 1, p. 016036, Jan. 2020, doi: 10.1088/1741-2552/AB581A.
- [29] “Projection :: Allen Brain Atlas: Mouse Connectivity.” <https://connectivity.brain-map.org/> (accessed Mar. 29, 2022).
- [30] “3d Viewer :: Allen Brain Atlas: Mouse Connectivity.” <https://connectivity.brain-map.org/3d-viewer?v=1> (accessed Mar. 29, 2022).
- [31] J. Peirce *et al.*, “PsychoPy2: Experiments in behavior made easy,” *Behavior Research Methods*, vol. 51, no. 1, pp. 195–203, Feb. 2019, doi: 10.3758/S13428-018-01193-Y/FIGURES/3.
- [32] C. M. Niell and M. P. Stryker, “Highly Selective Receptive Fields in Mouse Visual Cortex,” *Journal of Neuroscience*, vol. 28, no. 30, pp. 7520–7536, Jul. 2008, doi: 10.1523/JNEUROSCI.0623-08.2008.
- [33] P. Reinagel, “Training rats using water rewards without water restriction,” *Frontiers in Behavioral Neuroscience*, vol. 12, p. 84, May 2018, doi: 10.3389/FNBEH.2018.00084/BIBTEX.
- [34] A. E. Urai, V. Aguillon-Rodriguez, I. C. Laranjeira, F. Cazes, Z. F. Mainen, and A. K. Churchland, “Citric Acid Water as an Alternative to Water Restriction for High-Yield Mouse Behavior,” *eNeuro*, vol. 8, no. 1, pp. 1–8, Jan. 2021, doi: 10.1523/ENEURO.0230-20.2020.
- [35] Z. v. Guo *et al.*, “Procedures for Behavioral Experiments in Head-Fixed Mice,” *PLOS ONE*, vol. 9, no. 2, p. e88678, Feb. 2014, doi: 10.1371/JOURNAL.PONE.0088678.
- [36] A. E. Horner *et al.*, “The touchscreen operant platform for testing learning and memory in rats and mice,” *Nature Protocols* 2013 8:10, vol. 8, no. 10, pp. 1961–1984, Sep. 2013, doi: 10.1038/nprot.2013.122.
- [37] A. C. Mar *et al.*, “The touchscreen operant platform for assessing executive function in rats and mice,” *Nat Protoc*, vol. 8, no. 10, p. 1985, Oct. 2013, doi: 10.1038/NPROT.2013.123.
- [38] N. A. Steinmetz *et al.*, “Neuropixels 2.0: A miniaturized high-density probe for stable, long-term brain recordings,” *Science (1979)*, vol. 372, no. 6539, Apr. 2021, doi: 10.1126/SCIENCE.ABF4588/SUPPL_FILE/ABF4888_MJAR_REPRODUCIBILITY_CHECKLIST.PDF.

- [39] C. Rossant *et al.*, “Spike sorting for large, dense electrode arrays,” *Nature Neuroscience* 2016 19:4, vol. 19, no. 4, pp. 634–641, Mar. 2016, doi: 10.1038/nn.4268.
- [40] D. L. Ringach, R. M. Shapley, and M. J. Hawken, “Orientation Selectivity in Macaque V1: Diversity and Laminar Dependence,” *Journal of Neuroscience*, vol. 22, no. 13, pp. 5639–5651, Jul. 2002, doi: 10.1523/JNEUROSCI.22-13-05639.2002.
- [41] S. B. Khanna and M. A. Smith, “Deciphering the Neuronal Population Code,” *Neural Engineering*, pp. 519–534, 2020, doi: 10.1007/978-3-030-43395-6_18.
- [42] K. H. Britten, M. N. Shadlen, W. T. Newsome, and J. A. Movshon, “The analysis of visual motion: a comparison of neuronal and psychophysical performance,” *Journal of Neuroscience*, vol. 12, no. 12, pp. 4745–4765, Dec. 1992, doi: 10.1523/JNEUROSCI.12-12-04745.1992.